# Chiral singlet superconductivity in the weakly correlated metal LaPt3P

**Pabitra Biswas**
STFC Rutherford Appleton Laboratory https://orcid.org/0000-0002-7367-5960
**Sudeep Ghosh** ( S.Ghosh@kent.ac.uk )
University of Kent https://orcid.org/0000-0002-3646-0629
**Jianzhou Zhao**
Singapore University of Technology and Design
**Daniel Mayoh**
University of Warwick https://orcid.org/0000-0002-7020-3263
**Nikolai Zhigadlo**
University of Bern https://orcid.org/0000-0001-7322-5874
**Xiaofeng Xu**
Nanyang Technological University
**Chris Baines**
Paul Scherrer Institute
**Adrian Hillier**
ISIS, Science and Technology Facilities Council, Rutherford Appleton Laboratory, Harwell Science and Innovation Campus, Oxfordshire, England OX11 0QX, United Kingdom
**Geetha Balakrishnan**
Department of Physics https://orcid.org/0000-0002-5890-1149
**Martin Lees**
University of Warwick https://orcid.org/0000-0002-2270-2295

**Article**

**Keywords:** topological superconductors (SCs), superconductivity

**Posted Date:** December 29th, 2020

**DOI:** https://doi.org/10.21203/rs.3.rs-125751/v1

**Version of Record:** A version of this preprint was published at Nature Communications on May 4th, 2021. See the published version at https://doi.org/10.1038/s41467-021-22807-8.

# Chiral singlet superconductivity in the weakly correlated metal $LaPt_3P$

P. K. Biswas,[1,*] S. K. Ghosh,[2,†] J. Z. Zhao,[3] D. A. Mayoh,[4] N. D. Zhigadlo,[5,6]
Xiaofeng Xu,[7] C. Baines,[8] A. D. Hillier,[1] G. Balakrishnan,[4] and M. R. Lees[4]

[1] *ISIS Pulsed Neutron and Muon Source, STFC Rutherford Appleton Laboratory, Harwell Campus, Didcot, Oxfordshire OX11 0QX, United Kingdom*
[2] *School of Physical Sciences, University of Kent, Canterbury CT2 7NH, United Kingdom*
[3] *Co-Innovation Center for New Energetic Materials, Southwest University of Science and Technology, Mianyang, 621010, China*
[4] *Physics Department, University of Warwick, Coventry, CV4 7AL, United Kingdom*
[5] *Laboratory for Solid State Physics, ETH Zurich, 8093 Zurich, Switzerland*
[6] *CrystMat Company, 8037 Zurich, Switzerland*
[7] *Department of Applied Physics, Zhejiang University of Technology, Hangzhou 310023,China*
[8] *Laboratory for Muon Spin Spectroscopy, Paul Scherrer Institute, CH-5232 Villigen PSI, Switzerland*

(Dated: December 10, 2020)

**Topological superconductors (SCs) are novel phases of matter with nontrivial bulk topology. They host at their boundaries and vortex cores zero-energy Majorana bound states, potentially useful in fault-tolerant quantum computation [1]. Chiral SCs [2] are particular examples of topological SCs with finite angular momentum Cooper pairs circulating around a unique chiral axis, thus spontaneously breaking time-reversal symmetry (TRS). They are rather scarce and usually feature triplet pairing: best studied examples in bulk materials are $UPt_3$ and $Sr_2RuO_4$ proposed to be $f$-wave and $p$-wave SCs respectively, although many open questions still remain [2]. Chiral triplet SCs are, however, topologically fragile with the gapless Majorana modes weakly protected against symmetry preserving perturbations in contrast to chiral singlet SCs [3, 4]. Using muon spin relaxation ($\mu$SR) measurements, here we report that the weakly correlated pnictide compound $LaPt_3P$ has the two key features of a chiral SC: spontaneous magnetic fields inside the superconducting state indicating broken TRS and low temperature linear behaviour in the superfluid density indicating line nodes in the order parameter. Using symmetry analysis, first principles band structure calculation and mean-field theory, we unambiguously establish that the superconducting ground state of $LaPt_3P$ is chiral $d$-wave singlet.**

Cooper pairs in conventional SCs, such as the elemental metals, form due to pairing of electrons by phonon-mediated attractive interaction into the most symmetric $s$-wave spin-singlet state [5]. In contrast, unconventional SCs defined as having zero average onsite pairing amplitude pose a pivotal challenge in resolving how superconductivity emerges from a complex normal state. They usually require a long-range interaction [6] and have lower symmetry Cooper pairs. A special class of unconventional SCs are the chiral SCs. A well established realization of a chiral $p$-wave triplet state is the $A$-phase of superfluid $He^3$ [7]. In addition to $UPt_3$ and $Sr_2RuO_4$, the heavy fermion SC $UTe_2$ is also proposed to be a chiral triplet SC [8]. The chiral singlet SCs are, however, extremely rare and are proposed to be realized within the hidden order phase of the strongly correlated heavy fermion SC $URu_2Si_2$ [9] and in the locally noncentrosymmetric material SrPtAs [10] with many unresolved issues.

$LaPt_3P$ is a member of the platinum pnictide family of SCs $APt_3P$ ($A$ = Ca, Sr and La) with a centrosymmetric primitive tetragonal structure [11]. Its $T_c$ = 1.1 K is significantly lower than its other two isostructural counterparts $SrPt_3P$ ($T_c$ = 8.4 K) and $CaPt_3P$ ($T_c$ = 6.6 K) [11] which are conventional Bardeen-Cooper-Schrieffer (BCS) SCs. Indications of the unconventional nature of superconductivity in $LaPt_3P$ come both from theory: first principles Migdal-Eliashberg-theory [12] and experiments: very low $T_c$, unsaturated resistivity up to room temperature and a weak specific heat jump at $T_c$ [11]. The chiral nature of superconductivity of $LaPt_3P$ with topologically protected Majorana Fermi-arc and Majorana flat-band, which we uncover here, fits nicely with these characteristics.

## Experimental results

We have performed a comprehensive analysis of the superconducting properties of $LaPt_3P$ using the $\mu$SR technique. Two sets of polycrystalline $LaPt_3P$ specimens, referred to here as sample-A (from Warwick, UK) and sample-B (from ETH, Switzerland), were synthesized at two different laboratories by completely different methods. Zero-field (ZF), longitudinal-field (LF), and transverse-field (TF) $\mu$SR measurements were performed on these samples at two different muon facilities: sample-A in the MUSR spectrometer at the ISIS Pulsed Neutron and Muon Source, UK, and sample-B in the LTF spectrometer at the Paul Scherrer Institut (PSI), Switzerland.

ZF-$\mu$SR measurements reveal spontaneous magnetic fields arising just below $T_c \approx 1.1$ K (example charcterization is shown by the zero-field-cooled magnetic susceptibility ($\chi$) data for sample-B on the right axis of Fig. 1**b**)

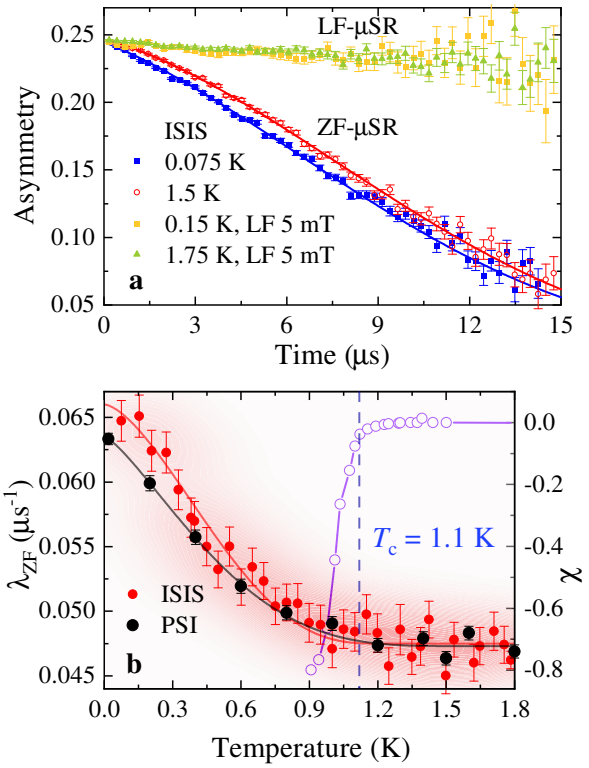


FIG. 1. **Evidence of TRS-breaking superconductivity in $LaPt_3P$ by ZF-$\mu$SR measurements.** **a**) ZF-$\mu$SR time spectra collected at 75 mK and 1.5 K for sample-A of $LaPt_3P$. The solid lines are the fits to the data using Eq. 1. **b**) The temperature dependence of the extracted $\lambda_{ZF}$ (left axis) for sample-A (ISIS) and sample-B (PSI) showing a clear increase in the muon spin relaxation rate below $T_c$. The PSI data has been shifted by 0.004 $\mu s^{-1}$ to match the baseline value of the ISIS data. Variation of the zero-field-cooled magnetic susceptibility ($\chi$) on the right axis for sample-B.

associated with a TRS breaking superconducting state in both samples of $LaPt_3P$, performed on different instruments. Fig. 1**a** shows representative ZF-$\mu$SR time spectra of $LaPt_3P$ collected at 75 mK (superconducting state) and at 1.5 K (normal state) on sample-A at ISIS. The data below $T_c$ show a clear increase in muon-spin relaxation rate compared to the data collected in the normal state. To unravel the origin of the spontaneous magnetism at low temperature, we collected ZF-$\mu$SR time spectra over a range of temperatures across $T_c$ and extracted temperature dependence of the muon-spin relaxation rate by fitting the data with a Gaussian Kubo-Toyabe relaxation function $\mathcal{G}(t)$ [13] multiplied by an exponential decay:

$$A(t) = A(0)\mathcal{G}(t)\exp(-\lambda_{ZF}t) + A_{bg} \quad (1)$$

where, $A(0)$ and $A_{bg}$ are the initial and background asymmetries of the ZF-$\mu$SR time spectra, respectively. $\mathcal{G}(t) = \frac{1}{3} + \frac{2}{3}\left(1 - \sigma_{ZF}^2 t^2\right)\exp\left(-\sigma_{ZF}^2 t^2/2\right)$. $\sigma_{ZF}$ and $\lambda_{ZF}$ represent the muon spin relaxation rates originating from the presence of nuclear and electronic moments in the sample, respectively. In the fitting, $\sigma_{ZF}$ is found to be nearly temperature independent and hence fixed to the average value of 0.071(4) $\mu s^{-1}$ for sample-A and 0.050(3) $\mu s^{-1}$ for sample-B. The temperature dependence of $\lambda_{ZF}$ is shown in Fig. 1**b**. $\lambda_{ZF}$ has a distinct systematic increase below $T_c$ for both the samples which implies that the effect is sample and spectrometer independent. Moreover, the effect can be suppressed very easily by a weak longitudinal field of 5 mT for both the samples. It is shown in Fig. 1**a** for sample-A. This strongly suggests that the additional relaxation below $T_c$ is not due to rapidly fluctuating fields [14], but rather associated with very weak fields which are static or quasistatic on the time-scale of muon life-time. The spontaneous static magnetic field arising just below $T_c$ is so intimately connected with superconductivity that we can safely say its existence is direct evidence for TRS-breaking superconducting state in $LaPt_3P$. From the change $\Delta\lambda_{ZF} = \lambda_{ZF}(T \approx 0) - \lambda_{ZF}(T > T_c)$ we can estimate the corresponding spontaneous internal magnetic field at the muon site $B_{int} \approx \Delta\lambda_{ZF}/\gamma_\mu = 0.22(4)$ G for sample-A and 0.18(2) G for sample-B which are very similar to that of other TRS breaking SCs [15]. Here, $\gamma_\mu/(2\pi) = 13.55$ kHz/G is the muon gyromagnetic ratio.

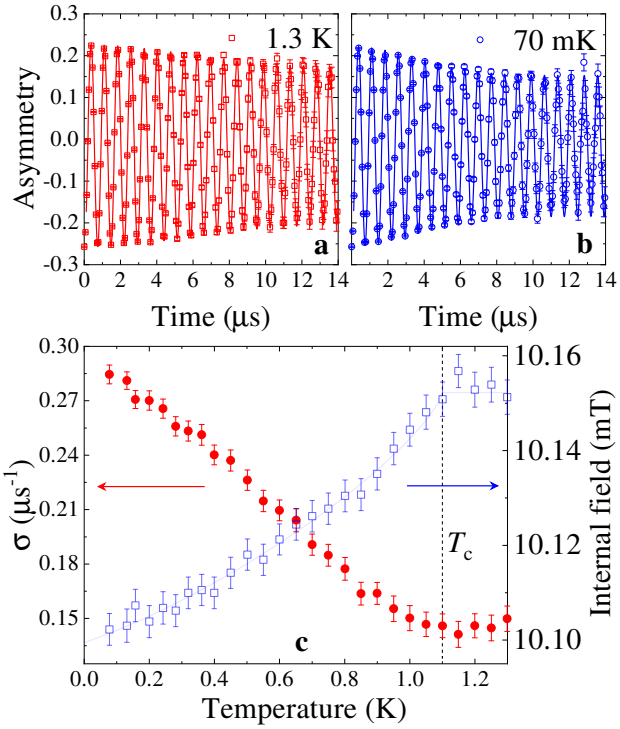


FIG. 2. **Superconducting properties of $LaPt_3P$ by TF-$\mu$SR measurements.** TF-$\mu$SR time spectra of $LaPt_3P$ collected at **a**) 1.3 K and **b**) 70 mK for sample-A in a transverse field of 10 mT. The solid lines are the fits to the data using Eq. 2. **c**) The temperature dependence of the extracted $\sigma$ (left panel) and internal field (right panel) of sample-A.

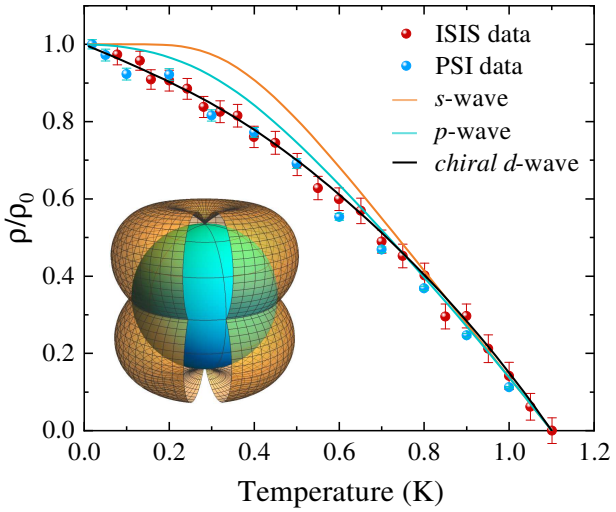


FIG. 3. **Evidence of *chiral d-wave* superconductivity in $LaPt_3P$.** Superfluid density ($\rho$) of $LaPt_3P$ as a function of temperature normalized by its zero-temperature value $\rho_0$. The solid lines are fits to the data using different models of gap symmetry. Inset shows the schematic representation of the nodes of the *chiral d-wave* state.

We show the TF-$\mu$SR time spectra for sample-A in Fig. 2**a** and Fig. 2**b** at two different temperatures. The spectrum in Fig. 2**a** shows only weak relaxation mainly due to the transverse (2/3) component of the weak nuclear moments present in the material in the normal state at 1.3 K. In contrast, the spectrum in Fig. 2**b** in the superconducting state at 70 mK shows higher relaxation due to the additional inhomogeneous field distribution of the vortex lattice, formed in the superconducting mixed state of $LaPt_3P$. The spectra are analyzed using the Gaussian damped spin precession function [13]:

$$A_{TF}(t) = A(0)\exp\left(-\sigma^2 t^2/2\right)\cos\left(\gamma_\mu \langle B\rangle t + \phi\right) + A_{\rm bg}\cos\left(\gamma_\mu B_{\rm bg} t + \phi\right). \quad (2)$$

Here $A(0)$ and $A_{\rm bg}$ are the initial asymmetries of the muons hitting and missing the sample respectively. $\langle B\rangle$ and $B_{\rm bg}$ are the internal and background magnetic fields, respectively. $\phi$ is the initial phase and $\sigma$ is the Gaussian muon spin relaxation rate of the muon precession signal. The background signal is due to the muons implanted on the outer silver mask where the relaxation rate of the muon precession signal is negligible due to very weak nuclear moments in silver. Fig. 2**c** shows the temperature dependence of $\sigma$ and internal field of sample-A. $\sigma(T)$ shows a change in slope at $T = T_{\rm c}$ which keeps on increasing with further lowering of temperature. Such an increase in $\sigma(T)$ just below $T_{\rm c}$ indicates that the sample is in the superconducting mixed state and the formation of vortex lattice has created an inhomogeneous field distribution at the muon sites. The internal fields felt by the muons show a diamagnetic shift in the superconducting state of $LaPt_3P$, a clear signature of bulk superconductivity in this material.

The true contribution of the vortex lattice field distribution to the relaxation rate $\sigma_{\rm sc}$ can be estimated as $\sigma_{\rm sc} = (\sigma^2 - \sigma_{\rm nm}^2)^{1/2}$, where $\sigma_{\rm nm} = 0.1459(4)\ \mu{\rm s}^{-1}$ is the nuclear magnetic dipolar contribution assumed to be temperature independent. Within the Ginzburg-Landau theory of the vortex state, $\sigma_{\rm sc}$ is related to the London penetration depth $\lambda$ of a SC with high upper critical field by the Brandt equation [16]:

$$\frac{\sigma_{sc}(T)}{\gamma_\mu} = 0.06091\frac{\Phi_0}{\lambda^2(T)}, \quad (3)$$

where $\Phi_0 = 2.068\times10^{-15}$ Wb is the flux quantum. The superfluid density $\rho \propto \lambda^{-2}$. Fig. 3 shows the temperature dependence of $\rho$ for $LaPt_3P$. It clearly varies with temperature down to the lowest temperature 70 mK and shows a linear increase below $T_{\rm c}/3$. This nonconstant low temperature behaviour is a signature of nodes in the superconducting gap.

The pairing symmetry of $LaPt_3P$ can be understood by analysing the superfluid density data using different models of the gap function $\Delta_{\boldsymbol{k}}(T)$. For a given pairing model, we compute the superfluid density ($\rho$) as

$$\rho = 1 + 2\left\langle \int_{\Delta_{\boldsymbol{k}}(T)}^{\infty} \frac{E}{\sqrt{E^2 - |\Delta_{\boldsymbol{k}}(T)|^2}}\frac{\partial f}{\partial E}dE\right\rangle_{\rm FS}. \quad (4)$$

Here, $f = 1/\left(1 + e^{\frac{E}{k_B T}}\right)$ is the Fermi function and $\langle\rangle_{\rm FS}$ represents an average over the Fermi surface (assumed to be spherical). We take $\Delta_{\boldsymbol{k}}(T) = \Delta_m(T)g(\boldsymbol{k})$ where we assume a universal temperature dependence $\Delta_m(T) = \Delta_m(0)\tanh\left[1.82\left\{1.018\left(T_{\rm c}/T - 1\right)\right\}^{0.51}\right]$ [17] and the function $g(\boldsymbol{k})$ contains its angular dependence. We use three different pairing models: *s*-wave (single uniform superconducting gap), *p*-wave (two point nodes at the two poles) and chiral *d*-wave (two point nodes at the two poles and a line node at the equator as shown in the inset of Fig. 3). The fitting parameters are given in the Supplemental Material. We note from Fig. 3 that both the *s*-wave and the *p*-wave models lead to saturation in $\rho$ at low temperatures which is clearly not the case for $LaPt_3P$ and the chiral *d*-wave model gives an excellent fit down to the lowest temperature. Nodal SCs are rare since the SC can gain condensation energy by eliminating nodes in the gap. Thus the simultaneous observation of nodal and TRS-breaking superconductivity makes $LaPt_3P$ a unique material.

## Discussion

We investigate the normal state properties of $LaPt_3P$ by a detailed band structure calculation using density functional theory within the generalized gradient approximation consistent with previous studies [12, 18]. $LaPt_3P$ is centrosymmetric with a paramagnetic normal state respecting TRS. It has significant effects of spin-orbit

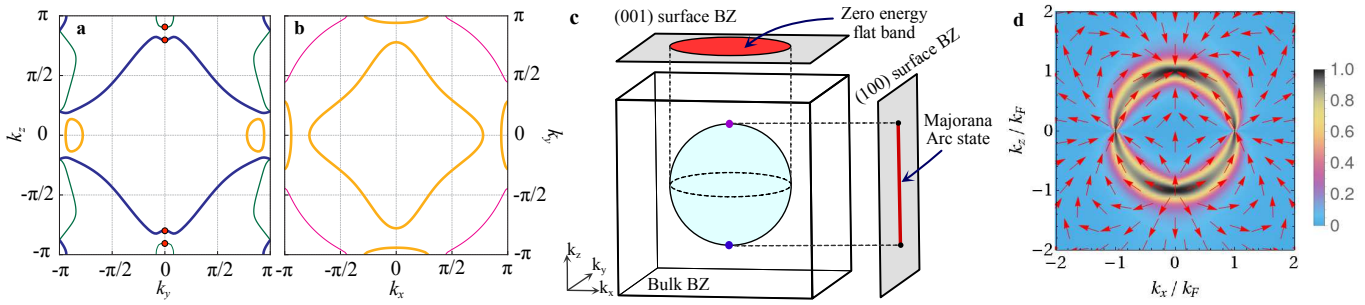


FIG. 4. **Properties of the normal and superconducting states of $LaPt_3P$.** Projections of the four Fermi surfaces of $LaPt_3P$ with SOC on the $y-z$ plane in **a** and $x-y$ plane in **b**. The thickness of the lines are proportional to the contribution of the Fermi surfaces to the DOS at the Fermi level (green– 10.3%, blue– 43.4%, orange– 40% and magenta– 6.3%). The point nodes of the *chiral d-wave* gap are shown by red dots in **a** and the line node reside on the $x-y$ plane in **b**. **c**) Schematic view of the Majorana Fermi-arc and the zero energy Majorana flat-band corresponding to the two Weyl point nodes and the line node respectively on the respective surface Brillouin zones (BZs) assuming a spherical Fermi surface. **d**) Berry curvature $\mathbf{F}(\boldsymbol{k})$ corresponding to the two Weyl nodes on the $x-z$ plane. Arrows show the direction of $\mathbf{F}(\boldsymbol{k})$ and the colour scale shows its magnitude $= \frac{2}{\pi}\arctan(|\mathbf{F}(\boldsymbol{k})|)$. $\Delta_0 = 0.5\mu$ was chosen for clarity while a more realistic weak-coupling limit $\Delta_0 \ll \mu$ gives a more sharply peaked curvature at the Fermi surface.

coupling (SOC) induced band splitting near the Fermi level ($\sim$ 120 meV, most apparent along the $MX$ high symmetry direction). Kramer's degeneracy survives in the presence of strong SOC due to centrosymmetry and SOC only produces small deformations in the Fermi surfaces [19]. The shapes of the Fermi surfaces play an important role in determining the thermodynamic properties of the material. The projections of the four Fermi surfaces of $LaPt_3P$ on the $y-z$ and $x-y$ plane are shown in Fig. 4**a** and Fig. 4**b** respectively with the Fermi surface sheets having the most projected-DOS at the Fermi level shown in blue and orange. It shows the multi-band nature of $LaPt_3P$ with orbital contributions mostly coming from the $5d$ orbitals of Pt and the $3p$ orbitals of P.

$LaPt_3P$ has a nonsymmorphic space group $P4/mmm$ (No. 129) with point group $D_{4h}$. From the group theoretical classification of the SC order parameters within the Ginzburg-Landau theory [15, 20], the only possible superconducting instabilities with strong SOC which can break TRS spontaneously at $T_c$ correspond to the two 2D irreducible representations, $E_g$ and $E_u$, of $D_{4h}$ [21]. The superconducting ground state in the $E_g$ channel is a pseudospin *chiral d-wave* singlet state with gap function $\Delta(\boldsymbol{k}) = \Delta_0 k_z(k_x + ik_y)$ where $\Delta_0$ is an amplitude independent of $\boldsymbol{k}$. While the $E_u$ order parameter is a pseudospin *nonunitary chiral p-wave* triplet state with $d$-vector $\boldsymbol{d}(\boldsymbol{k}) = [c_1 k_z, ic_1 k_z, c_2(k_x + ik_y)]$ where $c_1$ and $c_2$ are material dependent real constants independent of $\boldsymbol{k}$.

We compute the quasi-particle excitation spectrum for the two TRS breaking states on a generic single band spherical Fermi surface using the Bogoliubov-de Gennes mean field theory [15, 20]. The chiral $d$-wave singlet state leads to an energy gap $= |\Delta_0||k_z|\sqrt{k_x^2 + k_y^2}$. It has a line node at the "equator" for $k_z = 0$ and two point nodes at the "north" and "south" poles (shown in Fig. 4**a**). The low temperature thermodynamic properties are, however, dominated by the line node because of its larger low energy DOS than the point nodes. The triplet state has an energy gap $= \sqrt{g(k_x,k_y) + 2c_1^2k_z^2 - 2|c_1||k_z|\sqrt{f(k_x,k_y) + c_1^2k_z^2}}$ where $f(k_x,k_y) = c_2^2(k_x^2 + k_y^2)$. It has only two point nodes at the two poles and no line nodes. Thus, the low temperature linear behaviour of the superfluid density of $LaPt_3P$ shown in Fig. 3 is only possible in the chiral $d$-wave state with a line node in contrast to the triplet state with only point nodes which will give a quadratic behaviour and saturation at low temperatures. Thus $LaPt_3P$ is one of the rare unconventional SCs for which we can unambiguously identify the superconducting order parameter. The point nodes and the line node for the chiral $d$-wave state on the Fermi surface sheets of $LaPt_3P$ are shown in Fig. 4**a** and Fig. 4**b**.

We now discuss the topological properties of the chiral $d$-wave state of $LaPt_3P$ based on a generic single-band spherical Fermi surface (chemical potential $\mu = k_F^2/(2m)$ where $k_F$ is the Fermi wave vector and $m$ is the electron mass) [7, 22]. However, topological protection of the nodes also ensures stability against multiband effects. The effective angular momentum of the Cooper pairs is $L_z = +1$ (in units of $\hbar$) with respect to the chiral $c$-axis. The equatorial line node acts as a vortex loop in momentum space [23] and is topologically protected by a 1D winding number $w(k_x,k_y) = 1$ for $k_x^2 + k_y^2 < k_F^2$ and $= 0$ otherwise. The nontrivial topology of the line node leads to two-fold degenerate zero-energy Majorana bound states in a flat band on the $(0,0,1)$ surface BZ as shown in Fig. 4**c**. As a result, there is a diverging zero-energy DOS leading to a zero-bias conductance peak (which can be really sharp [24]) measurable in STM. This inversion

symmetry protected line node is extra stable due to even parity SC [3, 24]. The point nodes on the other hand are Weyl nodes and are impossible to gap out by symmetry-preserving perturbations. They act as a monopole and an anti-monopole of Berry flux as shown in Fig. 4**d** and are characterized by a $k_z$ dependent topological invariant, the sliced Chern number $C(k_z) = L_z$ for $|k_z| < k_F$ with $k_z \neq 0$ and $= 0$ otherwise (see the Supplemental Material for details). As a result, the $(1, 0, 0)$ and $(0, 1, 0)$ surface BZs each have a Majorana Fermi arc which can be probed by STM as shown in Fig. 4**c**. There are two-fold degenerate chiral surface states with linear dispersion carrying surface currents leading to local magnetisation that may be detectable using SQUID magnetometry. One of the key signatures of chiral edge states is the anomalous thermal Hall effect (ATHE) which depends on the length of the Fermi arc in this case. Impurities in the bulk can, however, increase the ATHE signal by orders of magnitude [25] over the edge contribution making it possible to detect with current experimental technology [26]. We also note that a 90° rotation around the $c$-axis for the chiral $d$-wave state leads to a phase shift of $\pi/2$ which can be measured by corner Josephson junctions [27].

*Acknowledgments*: PKB gratefully acknowledges the ISIS Pulsed Neutron and Muon Source of the UK Science & Technology Facilities Council (STFC) and Paul Scherrer Institut (PSI) in Switzerland for access to the muon beam times. SKG acknowledges the Leverhulme Trust for support through the Leverhulme early career fellowship. The work at the University of Warwick was funded by EPSRC,UK, Grant EP/T005963/1. XX is partially supported by the National Natural Science Foundation of China (Grants 11974061, U1732162). NDZ thanks K. Povarov and acknowledges support from the Laboratory for Solid State Physics, ETH Zurich where synthesis studies were initiated.

## METHODS

### $\mu$SR TECHNIQUE

$\mu$SR is a very sensitive microscopic probe to detect the local-field distribution within a material. This technique has been widely used to search for very weak fields (of the order of a fraction of a gauss) arising spontaneously in the superconducting state of TRS breaking SCs. The other great use of this technique is to measure the value and temperature dependence of the London magnetic penetration depth, $\lambda$, in the vortex state of type-II SCs [28]. $1/\lambda^2(T)$ is in turn proportional to the superfluid density which can provide direct information on the nature of the superconducting gap. Details of the $\mu$SR technique are given in the Supplemental Material.

### SAMPLE PREPARATION AND CHARACTERISATION

Two sets of polycrystalline samples (referred to as sample-A and sample-B) of $LaPt_3P$ were synthesized at two different laboratories (Warwick, UK and PSI, Switzerland) by completely different methods. While, sample-A was synthesized by solid state reaction method, sample-B was synthesized using the cubic anvil high-pressure and high-temperature technique. Details of the sample preparation and characterization are given in the Supplemental Material.

### DFT CALCULATION

The first principles density functional theory (DFT) calculations were performed by the full potential linearized augmented plane wave method implemented in the WIEN2k package [29]. The generalized gradient approximation with the Perdew-Burke-Ernzerhof realization was used for the exchange-correlation functional. The plane wave cutoff $K_{max}$ is given by $R_{mt} * K_{max} = 8.0$. For the self-consistent calculations, the BZ integration was performed on a Γ-centered mesh of $15 \times 15 \times 15$ k-points.

### Data availability

All the datasets that support the findings of this study are available from the corresponding author upon reasonable request. The ISIS DOI for our MUSR source data is https://doi.org/10.5286/ISIS.E.RB1720467.

* pabitra.biswas@stfc.ac.uk
† S.Ghosh@kent.ac.uk

[1] M. Sato and Y. Ando, "Topological superconductors: a review," Reports on Progress in Physics **80**, 076501 (2017).
[2] C. Kallin and J. Berlinsky, "Chiral superconductors," Reports on Progress in Physics **79**, 054502 (2016).
[3] S. Kobayashi, K. Shiozaki, Y. Tanaka, and M. Sato, "Topological Blount's theorem of odd-parity superconductors," Physical Review B **90**, 024516 (2014).
[4] P. Goswami and A. H. Nevidomskyy, "Topological Weyl superconductor to diffusive thermal Hall metal crossover in the B-phase of $UPt_3$," Physical Review B **92**, 214504 (2015).
[5] M. Tinkham, *Introduction to Superconductivity* (McGraw-Hill Inc., 1996).
[6] D. J. Scalapino, "A common thread: The pairing interaction for unconventional superconductors," Reviews of Modern Physics **84**, 1383 (2012).

[7] A. P. Schnyder and P. M. R. Brydon, "Topological surface states in nodal superconductors," Journal of Physics: Condensed Matter **27**, 243201 (2015).

[8] L. Jiao, S. Howard, S. Ran, Z. Wang, J. O. Rodriguez, M. Sigrist, Z. Wang, N. P. Butch, and V. Madhavan, "Chiral superconductivity in heavy-fermion metal $UTe_2$," Nature **579**, 523–527 (2020).

[9] J. A. Mydosh and P. M. Oppeneer, "Colloquium: Hidden order, superconductivity, and magnetism: The unsolved case of $URu_2Si_2$," Reviews of Modern Physics **83**, 1301–1322 (2011).

[10] P. K. Biswas, H. Luetkens, T. Neupert, T. Stürzer, C. Baines, G. Pascua, A. P. Schnyder, M. H. Fischer, J. Goryo, M. R. Lees, *et al.*, "Evidence for superconductivity with broken time-reversal symmetry in locally noncentrosymmetric SrPtAs," Physical Review B **87**, 180503 (2013).

[11] T. Takayama, K. Kuwano, D. Hirai, Y. Katsura, A. Yamamoto, and H. Takagi, "Strong coupling superconductivity at 8.4 K in an antiperovskite phosphide $SrPt_3P$," Physical Review Letters **108**, 237001 (2012).

[12] A. Subedi, L. Ortenzi, and L. Boeri, "Electron-phonon superconductivity in $A\mathrm{Pt}_3\mathrm{P}$ ($A$ = Sr, Ca, La) compounds: From weak to strong coupling," Physical Review B **87**, 144504 (2013).

[13] A. Yaouanc and P. D. De Reotier, *Muon spin rotation, relaxation, and resonance: applications to condensed matter*, Vol. 147 (Oxford University Press, 2011).

[14] R. S. Hayano, Y. J. Uemura, J. Imazato, N. Nishida, K. Nagamine, T. Yamazaki, Y. Ishikawa, and H. Yasuoka, "Spin fluctuations of itinerant electrons in MnSi studied by muon spin rotation and relaxation," Journal of the Physical Society of Japan **49**, 1773–1783 (1980).

[15] S. K. Ghosh, M. Smidman, T. Shang, J. F. Annett, A. D. Hillier, J. Quintanilla, and H. Yuan, "Recent progress on superconductors with time-reversal symmetry breaking," Journal of Physics: Condensed Matter **33**, 033001 (2020).

[16] E. H. Brandt, "Properties of the ideal Ginzburg-Landau vortex lattice," Physical Review B **68**, 054506 (2003).

[17] A. Carrington and F. Manzano, "Magnetic penetration depth of $MgB_2$," Physica C: Superconductivity **385**, 205–214 (2003).

[18] H. Chen, X. Xu, C. Cao, and J. Dai, "First-principles calculations of the electronic and phonon properties of $A\mathrm{Pt}_3\mathrm{P}$ ($A$ = Ca, Sr, and La): Evidence for a charge-density-wave instability and a soft phonon," Physical Review B **86**, 125116 (2012).

[19] S. Yip, "Noncentrosymmetric superconductors," Annu. Rev. Condens. Matter Phys. **5**, 15–33 (2014).

[20] M. Sigrist and K. Ueda, "Phenomenological theory of unconventional superconductivity," Reviews of Modern physics **63**, 239 (1991).

[21] Nonsymmorphic symmetries can give rise to additional symmetry-required nodes (other than the point group symmetry-required ones) on the Brillouin zone boundaries along the high symmetry directions. The nonsymmorphic symmetries of $LaPt_3P$, however, can only generate additional point nodes for the $E_g$ order parameter but no additional nodes for the $E_u$ case [30].

[22] P. Goswami and L. Balicas, "Topological properties of possible Weyl superconducting states of $URu_2Si_2$," arXiv preprint arXiv:1312.3632 (2013).

[23] T. T. Heikkilä, N. B. Kopnin, and G. E. Volovik, "Flat bands in topological media," JETP Letters **94**, 233 (2011).

[24] S. Kobayashi, Y. Tanaka, and M. Sato, "Fragile surface zero-energy flat bands in three-dimensional chiral superconductors," Physical Review B **92**, 214514 (2015).

[25] V. Ngampruetikorn and J. A. Sauls, "Impurity-induced anomalous thermal Hall effect in chiral superconductors," Physical Review Letters **124**, 157002 (2020).

[26] M. Hirschberger, R. Chisnell, Y. S. Lee, and N. P. Ong, "Thermal Hall effect of spin excitations in a kagome magnet," Physical Review Letters **115**, 106603 (2015).

[27] J. D. Strand, D. J. Van Harlingen, J. B. Kycia, and W. P. Halperin, "Evidence for complex superconducting order parameter symmetry in the low-temperature phase of $UPt_3$ from Josephson interferometry," Physical Review Letters **103**, 197002 (2009).

[28] J. E. Sonier, J. H. Brewer, and R. F. Kiefl, "$\mu$SR studies of the vortex state in type-II superconductors," Reviews of Modern Physics **72**, 769 (2000).

[29] P. Blaha, K. Schwarz, F. Tran, R. Laskowski, G. K. H. Madsen, and L. D. Marks, "WIEN2k: An APW+lo program for calculating the properties of solids," The Journal of Chemical Physics **152**, 074101 (2020).

[30] S. Sumita and Y. Yanase, "Unconventional superconducting gap structure protected by space group symmetry," Physical Review B **97**, 134512 (2018).

# Figures

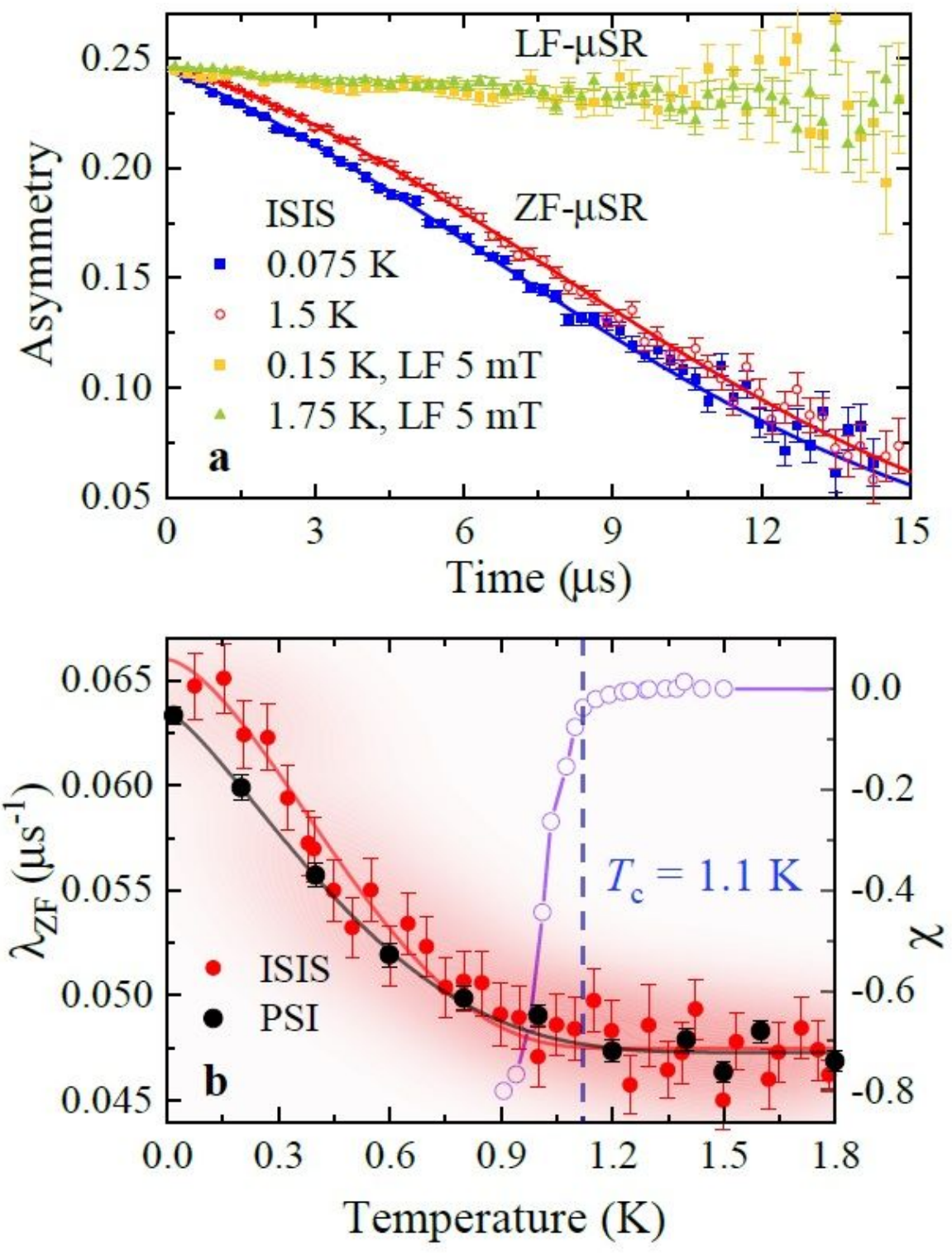


**Figure 1**

Evidence of TRS-breaking superconductivity in LaPt3P by ZF-uSR measurements. (see manuscript file for full legend)

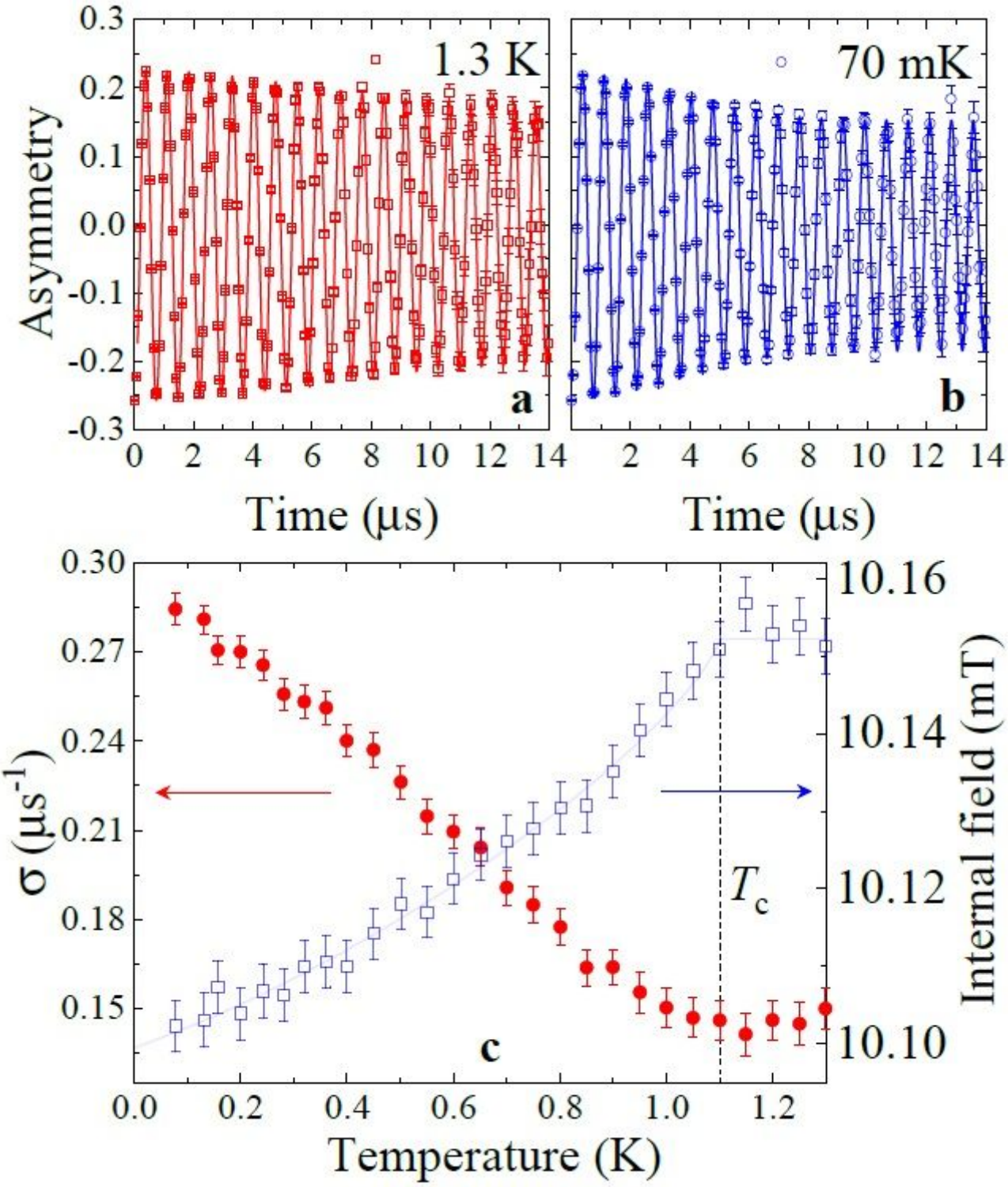


**Figure 2**

Superconducting properties of LaPt3P by TF-uSR measurements. (see manuscript file for full legend)

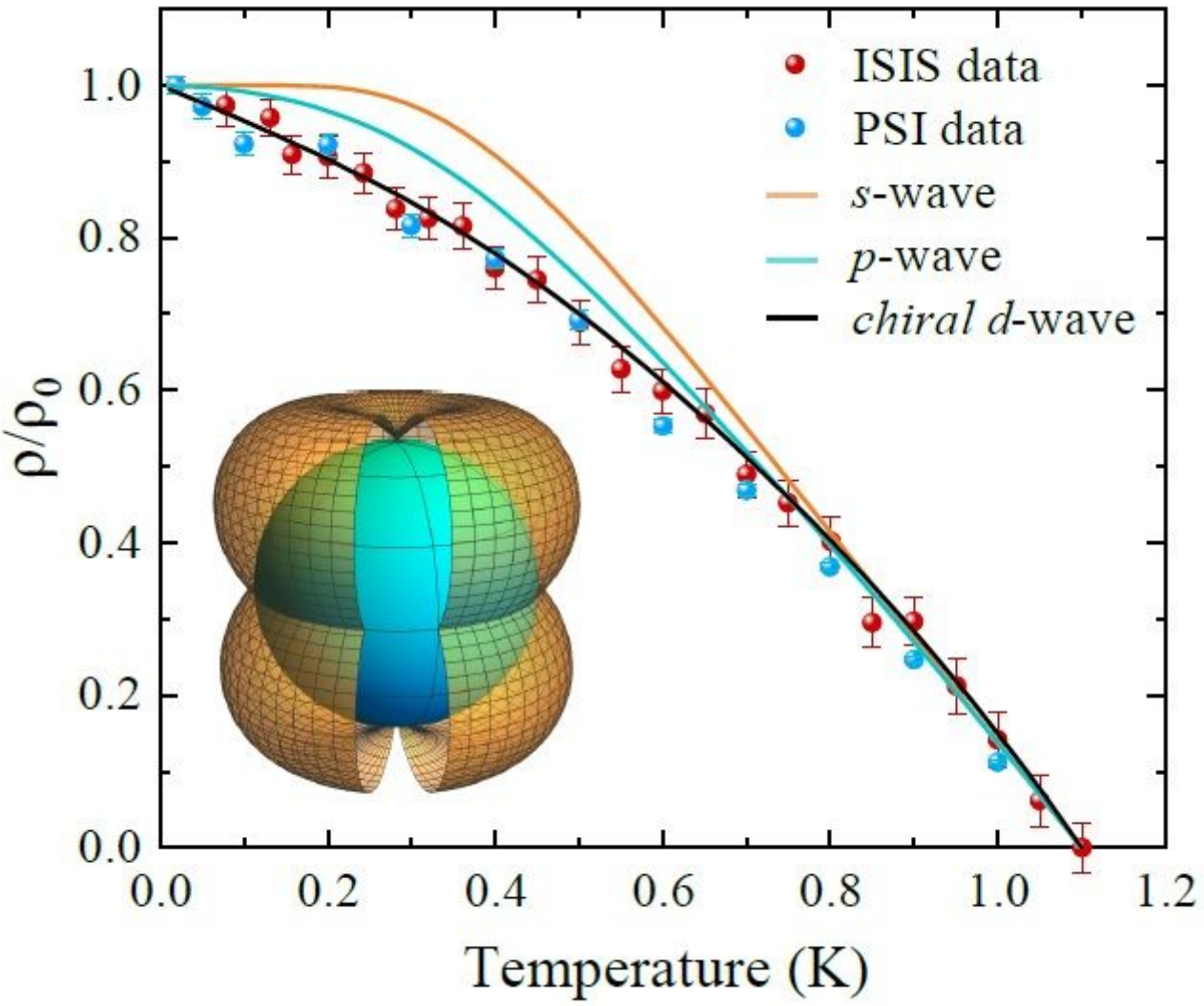


**Figure 3**

Evidence of chiral d-wave superconductivity in LaPt3P. (see manuscript file for full legend)

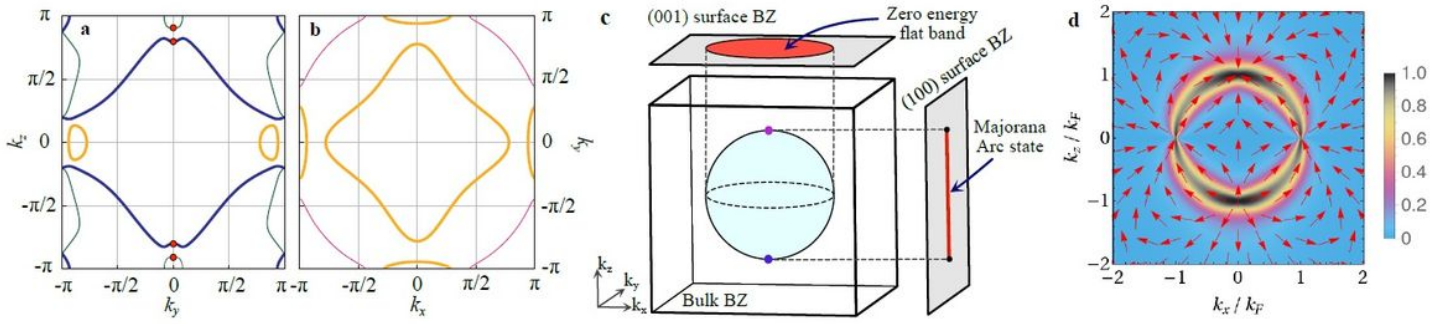


**Figure 4**

Properties of the normal and superconducting states of LaPt3P. (see manuscript file for full legend)

## Supplementary Files

This is a list of supplementary files associated with this preprint. Click to download.

- LaPt3PSMv06.pdf